# Transient Stability Evaluation of Benin Sub-Regional 330kV Grid Network Using Fletcher-Reeves Back Propagation Algorithm

Chizindu Stanley Esobinenwu
Department of Electrical/Electronic Engineering,
University of Port Harcourt, Rivers State, Nigeria

**Abstract.** Transient stability of Benin Sub-Region 330kV power system was examined using an artificial intelligent algorithm known as Fletcher-Reeves back propagation. Transient stability in recent times has become a huge challenge to power system engineers and operator. The system was first analyzed using modified Euler technique to compute the swing equation and plot the swing curve. Artificial neural network technique shows greater accuracy and speed in solving complex solution than the empirical method. Based on the result obtained, the maximum power outputs for pre-fault, during fault and post-fault condition are [2.2105, 0.6549, and 1.5672] respectively. Similarly, the critical clearing angle and time of the circuit breaker are [77.22 deg, 0.2 seconds] for the empirical method and [77.22 deg, 0.22 seconds] ANN methods. During ANN training the best validation performance is 0.00018754 at epoch 5, while the regression plot is 0.9993. It indicates how much minimized errors occurred during the training and the network procedure of training, testing and validation is significantly acceptable. Transient stability was improved with the use of circuit breaker.

**Key words:** Critical clearing time, Critical Clearing angle, Modified Euler, Circuit breaker, ANN

## 1.0 Introduction

A power system duly analyzed under a given operating state could be said to be stable if it maintains acceptable operating condition under normal and after being subjected to a disturbance.

Transient stability analysis in recent times has become a major challenge in power system operation (Wood, 2016).

According to Stevenson (2018), the indispensable condition under which a perfect network can be operated on is that all synchronous electrical machines must operate in optimal synchronization under steady state condition.

In stability studies, the main concern is the response of the system when it is faced with appropriate transient disturbance. It may be a very minute or almost negligible disturbance which could be due to load changing conditions or of large value ranging from short-circuit on transmission networks or very obvious and conspicuous disturbances such as loss of large load or generator or may be occurring as breakage of tie-line between two possible sub-systems (Odia, 2007).

The Nigerian 330kV power system network due to its lack of flexibility is highly stressed and operates closer to its capacity limits due to economic and environmental constraints.

Consequently, experiences a high rate of instability. In order to improve the system, an evaluation of the 330kV grid network is required to ascertain its ability to withstand disturbance while maintaining quality of service.

Currently, power system has modernized with the state of art infrastructure and digital computers. Hence, the need for the deployment of artificial intelligent in solving complex solution in power system becomes inevitable for system engineers. By this way, solution of network problem becomes easier unlike the use of empirical methods (Hague, 2012).

Artificial intelligence if fully deployed in power system can successfully solve complex challenging problems. According to Rastgoufard (2018), the main advantages of AI tools are their speed, robustness, and relative insensitivity to noisy or missing data. This paper present the use of artificial intelligent to determine the critical clearing time of circuit breaker required to eliminate three phase fault in a transmission line.

## 2.0 Literature Review

Prabha et al. (2014) defined stability as the capability of a network consisting of several interconnected synchronous machines to be consistent and retain its synchronism in spite of the fact that it has undergone or confronted by a disturbance. Furthermore, it was also aptly indicated that rotor angle instability may be associated with a retrogressive decrease in bus voltage. Consequently, the quantitative evaluation of rotor angles between two groups of machines may even approach values as much as 180 degrees, owing to loss of synchronism which causes a rapid drop in voltage at an intermediate position located in the network that is near to the electrical load concentrated center.

According to Gupta (2016), dynamic stability, in the context of electrical power networks, may be succinctly expressed as the capability of a power system to persist in the state of synchronism after experiencing transient stability pending when the system establishes back to new eventual steady (normal) state condition.

In his thesis, Enemuoh (2012) noted that maintaining synchronism in a typical power system is dependent on two realistic factors, which include damping and synchronizing torque. He further revealed that insufficient torques can lead to periodic or oscillatory instability.

Schlabbach and Rafalski (2008) reviewed that for an interconnected power system to work in stable manner, it should be capable of withstanding a wide range of contingency events in order to minimize cascading of faults. Frequency tolerance criteria must be fulfilled.

According to Barsha and Chin (2016), frequency stability may be briefly explained as the quality of a power system to constantly remain in its steady state frequency notwithstanding the level of upset it is attacked with. This may lead to inequality between power generation and load consumption values. The authors highlighted the major cause of frequency instability in the form of generation losses, which result in sudden unbalanced generating capacity in relation to consumption of load.

## 3.0 Methodology

### I. Data Collection

**Table 1. Load data**

| S/N | Load ID | Rated MVA | Shunt Mvar |
|---|---|---|---|
| 1 | Aladja TS | 180 | |
| 2 | Alaoji TS | 280 | 75 |
| 3 | Aliade TS | 120 | |
| 4 | Asaba TS | 100 | |
| 5 | Benin North TS | 80 | |
| 6 | Benin TS | 300 | 75,75 |
| 7 | Ikot Ekpene TS | 180 | |
| 8 | New Heaven TS | 200 | |
| 9 | Onitsha TS | 150 | 75 |
| 10 | Ugwaji TS | 200 | |

**Table 2. Generator data**

| S/n | Generating Station | | Capacity MW |
|---|---|---|---|
| | Name | Type | |
| 1 | Afam | Gas/Steam | 966 |
| 2 | Alaoji | Gas | 1074 |
| 3 | Delta | Gas | 480 |
| 4 | Ihovbor | Gas | 451 |
| 5 | Odukpani | Gas | 563 |
| 6 | Okpai | Gas/Steam | 480 |
| 7 | Sapele | Steam | 776 |

**Table 3. Line data**

| Transmission Line | | | Admittance |
|---|---|---|---|
| KM | From | To | Y(p.u) |
| 55 | Alaoji | IkotEkpene | 1.637-j2.626 |
| 137 | Benin | Onitsha | 5.848-j4.184 |
| 120 | Odukpani GS | IkotEkpene | 2.754-j3.553 |
| 70.3 | Ikot Ekpene | Ugwuaji | 2.754-j3.553 |
| 162 | Benin | Asaba | 6.494-j3.891 |
| 137 | Afam GS | Alaoji | 5.848-j4.184 |
| 25 | Afam GS | IkotEkpene | 2.754-j3.553 |
| 65 | Delta GS | Aladja | 6.494-j3.891 |
| 30 | Delta GS | Benin | 6.129-j9.615 |
| 107 | New Heaven | Ugwaji | 4.545-j3.247 |
| 6.5 | Odukpani GS | Adiabor | 1.637-j2.626 |
| 17.7 | Okpai GS | Onitsha | 1.192-j0.848 |
| 56 | Benin North | Onitsha | 1.192-j0.848 |
| 65.8 | Sapele GS | Benin | 1.923-j6.456 |
| 50 | Sapele GS | Aladja | 6.494-j3.891 |
| 63 | Asaba | Onitsha | 6.494-j3.891 |
| 65.8 | Onitsha | New Haven | 2.695-j1.919 |
| 96 | Onitsha | Alaoji | 0.246-j3.092 |
| 138 | Ugwuaji | Aliade | 2.695-j1.919 |
| 157 | Ihovbor GS | Benin | 6.494-j3.891 |

## II. Description of Study Area

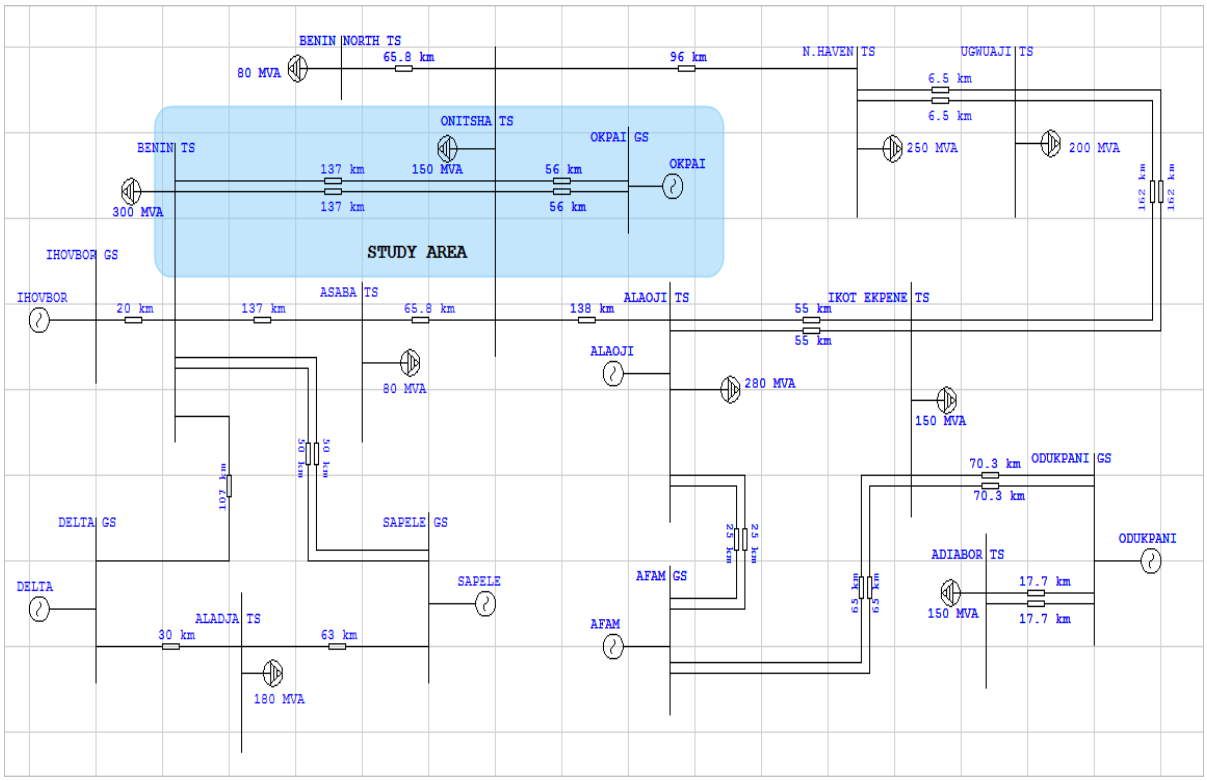


**Figure 1. Existing Nigerian Integrated 330KV Grid Network**

The Benin regional grid network covers states within the southern and eastern geographic region with Benin as the control centers. The control center is responsible for monitoring grid operations in all the 330kV and 132kV transmission network under the regional operations coordinating units shown in Figure 1.

## III. Formulation of the Swing Equation

The swing equation is used to describe the behavior of a synchronous machine during transient. It is a differential equation that relates the angular momentum M, the accelerating power $P_a$ and the rotor angle δ of the machine.

The kinetic energy of the rotor is given by

$$J = mr^2 \quad (1)$$

$$K_e = \frac{1}{2}J\omega^2 \quad (2)$$

$$M = J\omega \quad (3)$$

$$K_e = \frac{1}{2}M\omega \quad (4)$$

H Constant is the kinetic energy stored in the rotating parts of the machine at synchronous speed per unit MVA.

$$H = \frac{K_e}{G} \quad (5)$$

Substituting $K_e$ from (4) into (5)

$$H = \frac{M\omega}{2G} \quad (6)$$

$$M = \frac{GH}{\pi f} = \frac{GH}{180f} \quad (7)$$

Rotor angular displacement and acceleration is given by

$$\omega = \frac{d\delta}{dt} \quad (8)$$

$$\alpha = \frac{d\omega}{dt} = \frac{d^2\delta}{dt^2} \quad (9)$$

Generator accelerating toque and power is given by

$$T_a = J\alpha = \frac{M\alpha}{\omega} \quad (10)$$

$$P_a = \omega T_a \quad (11)$$

$$P_a = M\alpha \quad (12)$$

Substituting $\alpha$ from (9) into (12)

$$P_a = M\frac{d^2\delta}{dt^2} \quad (13)$$

$$P_a = P_s - P_e \quad (14)$$

$$M\frac{d^2\delta}{dt^2} = P_s - P_e \quad (15)$$

Where
r= radius of gyration in kg-m$^2$
m= mass of rotor in kg
$\omega$= synchronous speed of the rotor in rad/s
$J$= moment of inertia of the rotor in kg-m$^2$
M= angular momentum of the rotor in MJs/elect radian or degree
$K_e$= kinetic energy of the rotor in MJ
G= Generator rating in MVA
H= Inertia Constant in MJ/MVA
f= Frequency in $H_z$
$P_s$= Mechanical power in Watts
$P_e$= Electrical power in Watts

## IV. Determination of Power Output

The output power of the generator supplying an infinite bus through a double circuit transmission line can be determined for pre-fault, during fault and post-fault condition.

### *I. Pre-Fault Condition*

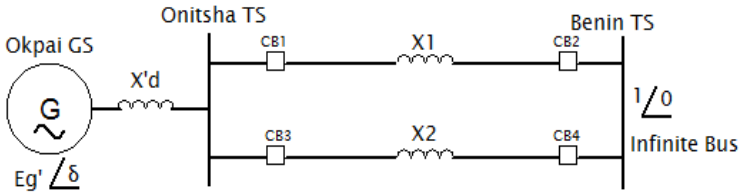


**Figure 2. Network without fault**

The transfer reactance of the line for pre-fault condition is given by

$$X_{eq1} = X'_d + \frac{X_1 X_2}{X_1 + X_2} \quad (16)$$

The output power transfer for pre-fault condition is given by

$$P_{m1} = \frac{E'_g V_1}{X_{eq1}} \quad (17)$$

$$P_{e1} = P_{m1} \sin \sigma_0 \quad (18)$$

Where
$X_1$= reactance of line 1
$X_2$= reactance of line 2
$X'd$= reactance of generator
$Pe_1$= output power

$Pm_1$= maximum power transfer before fault
$E'g$= generator emf or internal voltage
$V_1$=terminal voltage

***II. During-Fault Condition***

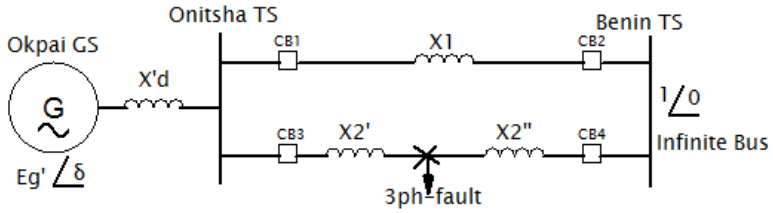


**Figure 3. Network with fault**

To determine the transfer reactance during fault condition, the line is first transformed from delta to star using delta-star transformation as shown in Figure 4 and finally from star-delta using star-delta transformation as shown in Figure 5.

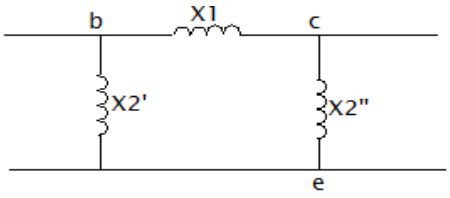


**Figure 4. Equivalent circuit for delta-star transformation**

$$X_b = \frac{X_1 X_{2'}}{X_1 + X_{2'} + X_{2''}} \quad (19)$$

$$X_c = \frac{X_1 X_{2''}}{X_1 + X_{2'} + X_{2''}} \quad (20)$$

$$X_e = \frac{X_{2'} X_{2''}}{X_1 + X_{2'} + X_{2''}} \quad (21)$$

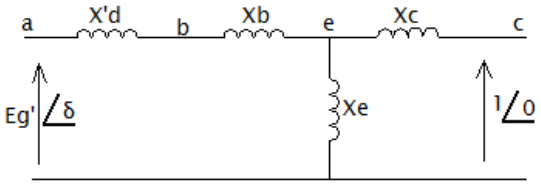


**Figure 5. Equivalent circuit for delta-star transformation**

$$X_a = Z'_g + X_b \quad (22)$$

$$X_{eq2} = X_a + X_c + \frac{X_a X_c}{X_e} \quad (23)$$

The output power transfer for during-fault condition is given by

$$P_{m2} = \frac{E'_g V_1}{X_{eq2}} \quad (24)$$

$$P_{e2} = P_{m2} \sin \sigma \quad (25)$$

***III. Post-Fault Condition***

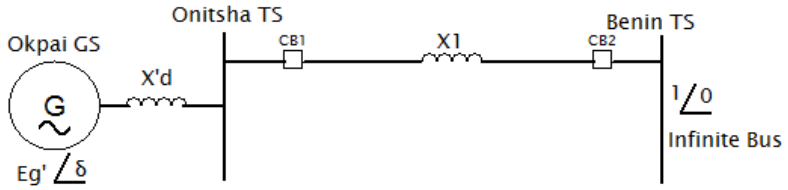


**Figure 6. Transmission line**

The transfer reactance of the line for post-fault condition is given by

$$X_{eq3} = X'_d + X_1 \quad (26)$$

The output power transfer for post-fault condition is given by

$$P_{m3} = \frac{E'_g V_1}{X_{eqs}} \quad (27)$$

$$P_{e3} = P_{m3} \sin \sigma_s \quad (28)$$

## V. Determination of Critical Clearing Angle

$$\sigma_{cc} = cos^{-1}\left[\frac{P_s(\sigma_m - \sigma_0) + P_{m3}cos\sigma_m - P_{m2}cos\sigma_0}{P_{m3} - P_{m2}}\right] \quad (29)$$

$$\sigma_0 = \sin^{-1}\left(\frac{P_{e1}}{P_{m1}}\right) \quad (30)$$

$$\sigma_s = \sin^{-1}\left(\frac{P_{es}}{P_{ms}}\right) \quad (31)$$

$$\sigma_m = \pi - \sigma_s \quad (32)$$

Where,
Ps= mechanical power input
$Pm_2$= maximum power transfer during fault
$Pm_3$= maximum power transfer after fault is cleared
$\sigma_{cc}$= Critical clearing angle in degree
$\sigma_0$= Power angle in degree

## VI. Determination of Critical Clearing Time

$$t_{cc} = \sqrt{\frac{2H(\delta_{cc} - \delta_0)}{\pi f P_s}} \quad (33)$$

Where,
$\sigma_{cc}$= Critical clearing angle in degree
$\sigma_0$= Power angle in degree
H= Inertia Constant in MJ/MVA
f= Frequency in $H_z$
$P_s$= Mechanical power in Watts

## VII. Numerical Solution of Swing Equation

The methods are used for solving swing equation are;
(i) Equal area criterion
(ii) Point by point method
(iii) Euler method
(iv) Lianupuv's direct method
(v) Modified Euler method
(vi) Runge-Kutta method

Among other methods, Modified Euler and Runge-Kutta are the two most popular used methods for solving swing equation. For this paper, Modified Euler's method was used due to its simplicity of technique and less computation time.

To determine the swing curve, the second order differential equation in (15) can be written as two first order differential equation and solution obtained using Modified Euler's method.

***I. Predictor Step***

Let $\delta_0$ and $\omega_0$be the initial point and $\Delta t$ the increment in time

$$\frac{d\delta}{dt}|_{t=t_0} = (\omega_0 - \omega_s) \quad (34)$$

$$\frac{d\omega}{dt}|_{t=t_0} = \frac{\pi f}{H}\left(P_s - P_e^{(0)}\right) \quad (35)$$

The approximate value of $\delta$ and $\omega$ denoted as $\delta^{(1)}$ and $\omega^{(1)}$ are calculated as follows:

$$\delta^{(1)} = \delta_0 + \Delta t \frac{d\delta}{dt}|_{t=t_0} \quad (36)$$

$$\delta^{(1)} = \delta_0 + \Delta t(\omega_0 - \omega_s) \quad (37)$$

$$\omega^{(1)} = \omega_0 + \Delta t \frac{d\omega}{dt}|_{t=t_0} \quad (38)$$

$$\omega^{(1)} = \omega_0 + \Delta t \frac{\pi f}{H}(P_s - P_e^{(0)}) \quad (39)$$

***II. Corrector Step***

With the new value of $\delta^{(1)}$ and $\omega^{(1)}$obtained in the predictor step, the value of $P_e$ denoted as $P_{ei}{}^{(1)}$ is updated.

$$\frac{d\delta}{dt}|_{t=t_0+\Delta t} = \left(\omega^{(1)} - \omega_s\right) \quad (40)$$

$$\frac{d\omega}{dt}|_{t=t_0+\Delta t} = \frac{\pi f}{H}\left(P_s - P_e^{(1)}\right) \quad (41)$$

With the above new derivative values obtained, the final value of $\delta$ and $\omega$at $t = t_0 + \Delta t$ denoted as $\delta_1$ and $\omega_1$ are calculated as

$$\delta_1 = \delta_0 + \frac{\Delta t}{2}\left[\frac{d\delta}{dt}|_{t=t_0} + \frac{d\delta}{dt}|_{t=t_0+\Delta t}\right] \quad (42)$$

$$\omega_1 = \omega_0 + \frac{\Delta t}{2}\left[\frac{d\omega}{dt}|_{t=t_0} + \frac{d\omega}{dt}|_{t=t_0+\Delta t}\right] \quad (43)$$

Proceeding further, for calculating $\delta$ and $\omega$ at $t = t_0 + 2\Delta t$, the initial points $\delta_0$ and $\omega_0$ are replaced by $\delta_1$ and $\omega_1$ respectively.

## VIII. Transient Stability Calculation

***Pre-fault condition***

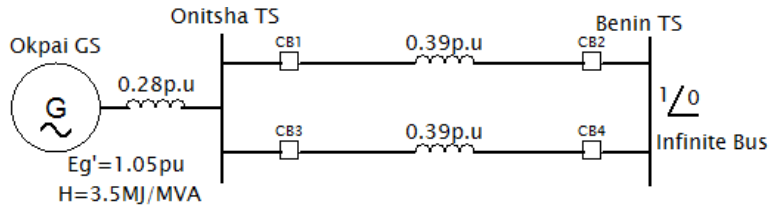


**Figure 7. Pre-fault condition**

From (16) the transfer reactance of the line in pre-fault condition is

$$X_{eq1} = 0.28 + \frac{0.39x0.39}{0.39 + 0.39} = 0.475p.u$$

From (17) and (18) the power transfer in pre-fault condition is

$$P_{m1} = \frac{1.05x1.0}{0.475} = 2.2105p.u$$
$$P_{e1} = 2.2105 \sin \sigma_0$$

***During-fault condition***

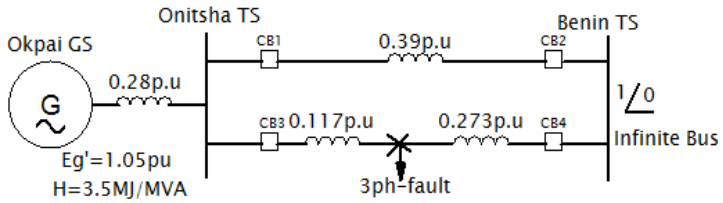


**Figure 8. During-fault condition**

From (19)-(23) the transfer reactance of the line during-fault condition is
Using delta-star transformation

$$X_b = \frac{0.39x0.117}{0.39 + 0.117 + 0.273} = 0.0585p.u$$
$$X_c = \frac{0.39x0.273}{0.39 + 0.117 + 0.273} = 0.1365p.u$$
$$X_e = \frac{0.117x0.273}{0.39 + 0.0117 + 0.273} = 0.04095p.u$$

Using star-delta transformation

$$X_a = 0.28 + 0.0585 = 0.3385p.u$$
$$X_{eq2} = 0.3385 + 0.1365 + \frac{0.3385x0.1365}{0.04095}$$
$$X_{eq2} = 1.6033p.u$$

From (24) and (25) the power transfer during-fault condition is

$$P_{m2} = \frac{1.05x1.0}{1.6033} = 0.6549p.u$$
$$P_{e2} = 0.6549 \sin \sigma$$

***Post-fault condition***

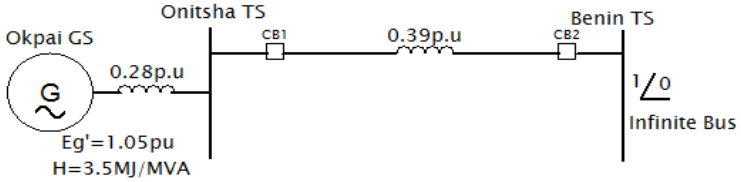


**Figure 9. Post-fault condition**

From (26) the transfer reactance of the line in post-fault condition is

$$X_{eq3} = 0.28 + 0.39 = 0.67p.u$$

The output power transfer for post-fault condition is given by

$$P_{m3} = \frac{1.05x1.0}{0.67} = 1.5672p.u$$
$$P_{e3} = 1.5672 \sin \sigma_s$$

## IX. Determination of Critical Clearing Angle

$$P_{e1} = P_{e3} = P_s = 1.0$$

Substituting these values in (30) and (31)

$$\sigma_0 = \sin^{-1}\left(\frac{1}{2.2105}\right) = 26.9° = 0.4694\ rad$$

$$\sigma_s = \sin^{-1}\left(\frac{1}{1.5672}\right) = 39.6° = 0.693\ rad$$

$$\sigma_m = \pi - \sigma_s => 180° - 39.6° = 140.4° = 2.450\ rad$$

$$\sigma_{cc} = cos^{-1}\left[\frac{P_s(\sigma_m - \sigma_0) + P_{m3}cos\sigma_m - P_{m2}cos\sigma_0}{P_{m3} - P_{m2}}\right]$$

$$\sigma_{cc} = cos^{-1}\left[\frac{1.0(2.450 - 0.469) + 1.5672xcos2.450 - 0.6549xcos0.469}{1.5762 - 0.6549}\right]$$

$$\sigma_{cc} = cos^{-1}\left[\frac{1.981 - 1.207 - 0.584}{0.9213}\right]$$

$$\sigma_{cc} = cos^{-1}\left[\frac{0.19}{0.9213}\right] = 1.3631\ rad = 78.1°$$

## X. Determination of Critical Clearing Time

The critical clearing time of fault is determine from (33) as

$$t_{cc} = \sqrt{\frac{2H(\delta_{cc} - \delta_0)}{\pi f P_s}} = \sqrt{\frac{2x3.5(1.363 - 0.469)}{3.142x50x1.0}}$$

$$t_{cc} = \sqrt{\frac{6.258}{157.1}} = 0.2sec$$

## XI. Artificial Neural Network Implementation in Transient Stability Study

The artificial neurons are similar to biological neurons in the way and manner they learn. Neural network learn through an iterative process during which input signals are modified by the weight of the neurons.

### *I. Neural Network Architecture*

The proposed neural network architecture shown in Figure 10 and 11 consist of three (3) layers.

**Input layer:** consist of three (3) neurons; inertial coefficient (M), Rotor angle and Output power

**Hidden layer:** consist of weights and bias which used to store information and modify the inputs during learning process.

**Output layer:** consist one (1) neuron and of functions that generates the target which is the critical clearing time. The output layer is also hidden.

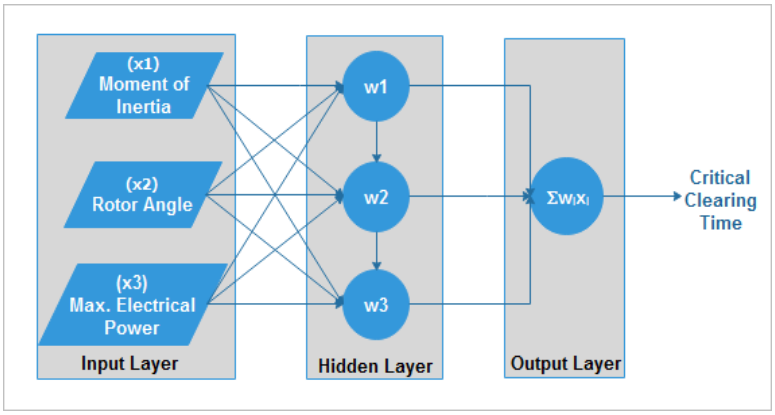


**Figure 10. Proposed Network Architecture**

### *II. ANN Training Process*

In Artificial Neural network training of network data is through an iterative process during which input signals are modified by the weight of the neurons until a perfect learning is achieved. At the point regression coefficient is approximately unity. Table 3 shows the training which consist of three input signals and one target.

**Table 3. Training data**

| Moment Inertial | Rotor Angle | Power Output | CCT |
|---|---|---|---|
| 0.009 | 26.89 | 0.709 | 0.00 |
| 0.009 | 27.23 | 0.832 | 0.02 |
| 0.009 | 28.49 | 0.948 | 0.04 |
| 0.009 | 31.21 | 1.057 | 0.06 |
| 0.009 | 35.19 | 1.157 | 0.08 |
| 0.009 | 39.24 | 1.247 | 0.10 |
| 0.009 | 44.17 | 1.328 | 0.12 |
| 0.009 | 50.78 | 1.397 | 0.14 |
| 0.009 | 60.39 | 1.456 | 0.16 |
| 0.009 | 70.66 | 1.502 | 0.18 |
| 0.009 | 77.22 | 1.536 | 0.20 |
| 0.009 | 80.37 | 1.558 | 0.22 |
| 0.009 | 79.35 | 1.567 | 0.24 |
| 0.009 | 76.67 | 1.563 | 0.26 |

$$\text{Inputs data} = \begin{bmatrix} M_1 & \delta_1 & Pe_1 \\ \vdots & \vdots & \vdots \\ M_n & \delta_n & Pe_n \end{bmatrix} \quad (44)$$

$$\text{Target data} = [cct_1, cct_2, cct_3\text{-------}cct_n] \quad (45)$$

$$Output\,(y) = \emptyset\left(\sum_{i=1}^{n} w_i x_i\right) \quad (46)$$

$$\text{Weight} = \begin{bmatrix} w_1 \\ w_2 \\ w_3 \end{bmatrix} \quad (47)$$

$$(y) = \frac{1}{1+e^{-((M_1 * W_1)+(\delta_2 * W_2)+(Pe_3 * W_3))}} \quad (48)$$

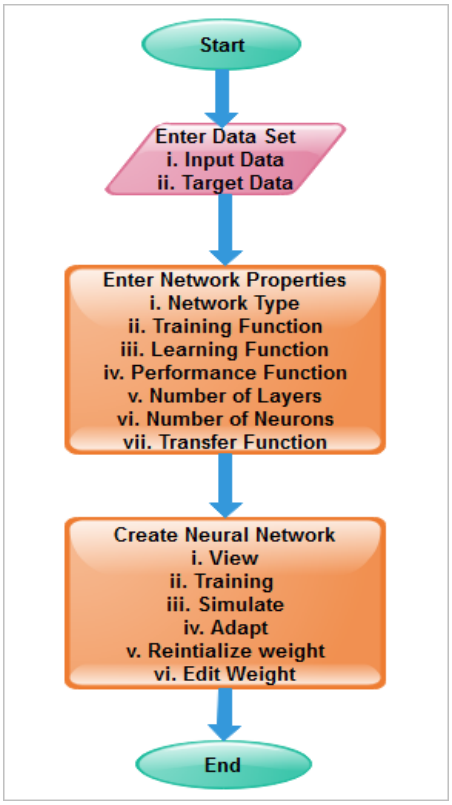


**Figure 11. ANN Training Flow Chart**

## 4.0 Result and Discussion

**Table 4. Power angle table**

| Pe1 | Pe2 | Pe3 | CCA |
|---|---|---|---|
| 1.000 | 0.296 | 0.709 | 26.900 |
| 1.174 | 0.348 | 0.832 | 32.068 |
| 1.338 | 0.396 | 0.948 | 37.236 |
| 1.491 | 0.442 | 1.057 | 42.404 |
| 1.632 | 0.483 | 1.157 | 47.572 |
| 1.759 | 0.521 | 1.247 | 52.741 |
| 1.873 | 0.555 | 1.328 | 57.909 |
| 1.971 | 0.584 | 1.397 | 63.077 |
| 2.053 | 0.608 | 1.456 | 68.245 |
| 2.119 | 0.628 | 1.502 | 73.413 |
| 2.167 | 0.642 | 1.536 | 78.581 |
| 2.197 | 0.651 | 1.558 | 83.749 |
| 2.210 | 0.655 | 1.567 | 88.917 |
| 2.205 | 0.653 | 1.563 | 94.085 |
| 2.182 | 0.646 | 1.547 | 99.253 |
| 2.141 | 0.634 | 1.518 | 104.422 |
| 2.083 | 0.617 | 1.477 | 109.590 |
| 2.007 | 0.595 | 1.423 | 114.758 |
| 1.916 | 0.568 | 1.358 | 119.926 |
| 1.809 | 0.536 | 1.282 | 125.094 |
| 1.687 | 0.500 | 1.196 | 130.262 |
| 1.551 | 0.460 | 1.100 | 135.430 |
| 1.403 | 0.416 | 0.995 | 140.598 |

Table 4 shows the power angle table for pre-fault, during fault and post fault condition. The system was first analyzed using modified Euler to solve the second order swing equation. The critical clearing angle and maximum output power was obtained.

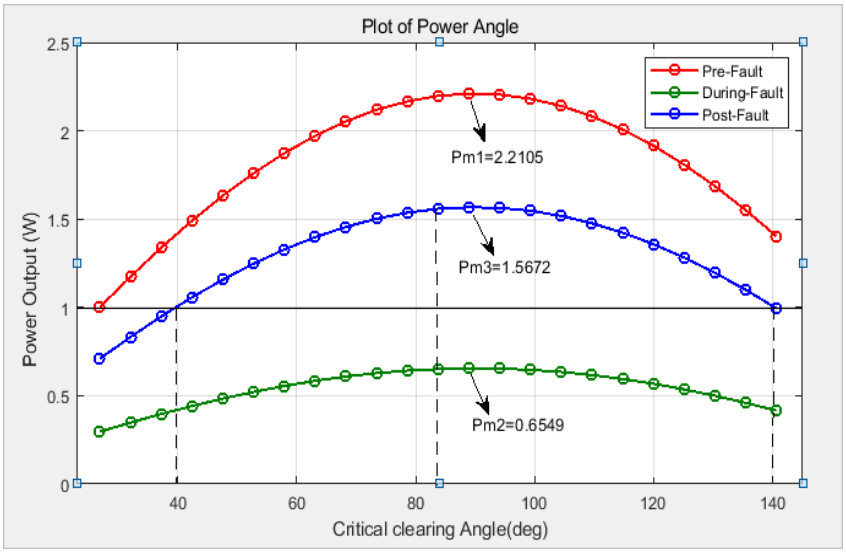


**Figure 12. Power angle plot**

Figure 12 shows plot of the power angle curve for pre-fault, during fault and post-fault condition. A quick look at the curve show that the maximum power output for pre-fault, during fault and post-fault condition are [2.2105, 0.6549, and 1.5672] respectively.

**Table 5. ANN result compared with empirical**

| Moment of Inertia | Power Pe2 | Rotor Angle | CCT(second) | |
|---|---|---|---|---|
| | | | Empirical | ANN |
| 0.009 | 0.709 | 26.89 | 0.00 | 0.01 |
| 0.009 | 0.832 | 27.23 | 0.02 | 0.02 |
| 0.009 | 0.948 | 28.49 | 0.04 | 0.04 |
| 0.009 | 1.057 | 31.21 | 0.06 | 0.07 |
| 0.009 | 1.157 | 35.19 | 0.08 | 0.08 |
| 0.009 | 1.247 | 39.24 | 0.10 | 0.09 |
| 0.009 | 1.328 | 44.17 | 0.12 | 0.13 |
| 0.009 | 1.397 | 50.78 | 0.14 | 0.15 |
| 0.009 | 1.456 | 60.39 | 0.16 | 0.16 |
| 0.009 | 1.502 | 70.66 | 0.18 | 0.21 |
| 0.009 | 1.536 | 77.22 | 0.20 | 0.22 |
| 0.009 | 1.558 | 80.37 | 0.22 | 0.22 |
| 0.009 | 1.567 | 79.35 | 0.24 | 0.22 |
| 0.009 | 1.563 | 76.67 | 0.26 | 0.22 |

Table 5 shows the output result from ANN training. The table consist of three (3) input neurons [moment of inertia, rotor angle and output power during fault condition. The critical clearing time of the circuit breaker was obtained and result compared for both ANN and Empirical method. A quick look at the table shows that the critical clearing time was 0.2 second.

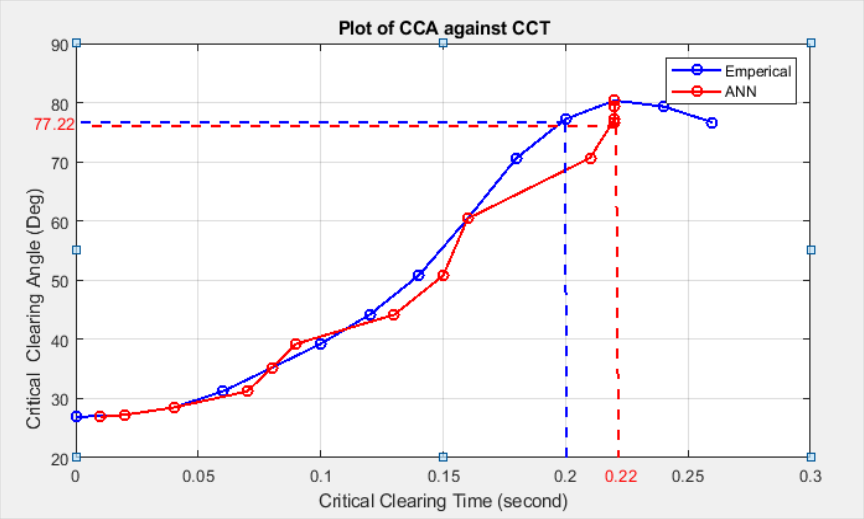


**Figure 13. Comparative plot of CCT**

Figure 13 show the comparative plot of the critical angle against critical clearing time. A quick look at the curve shows that the critical clearing angle of the circuit breaker is 77.22 for both empirical and ANN methods. While the critical clearing time is 0.2 second for empirical and 0.22 for ANN methods.

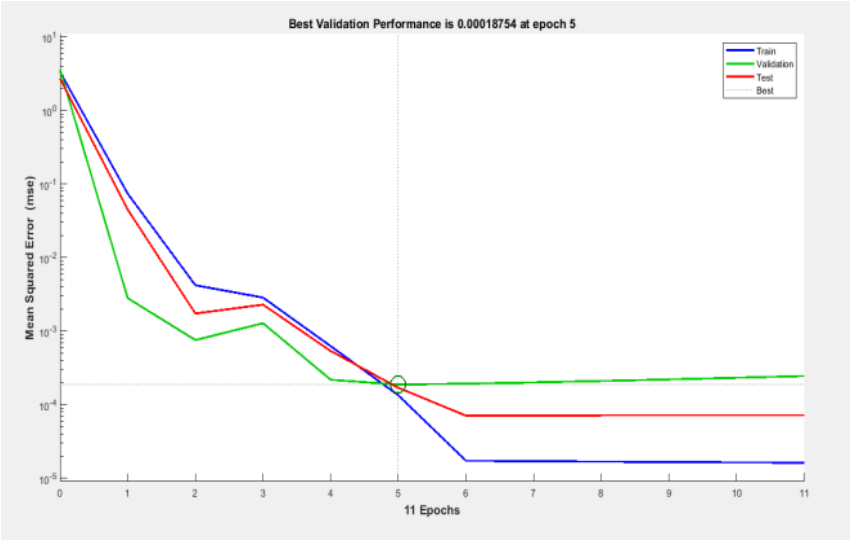


**Figure 14. Plot of ANN Training Performance**

Figure 14 shows the performance of the training process. During training, the performance for each iteration is computed and the point of intersection of the three line is chosen as the best performance. A quick look at Figure 14 shows that the best validation performance during training process is 0.00018754 at epoch 5 which indicates how much minimized errors occurred during the training.

Figure 15 shows the regression plot of the output network against the targets. The plot reveals that the fitness of the training data. The dash line represents the target while the solid line represents the best linear regression line between output and targets. The values of R = 1 shows there is a linear relationship between outputs and targets. A quick look at Figure 15 shows the R value equals to 0.9993. This shows the network procedure of training, testing and validation are significantly acceptable and a perfect regression existed between the output and the target.

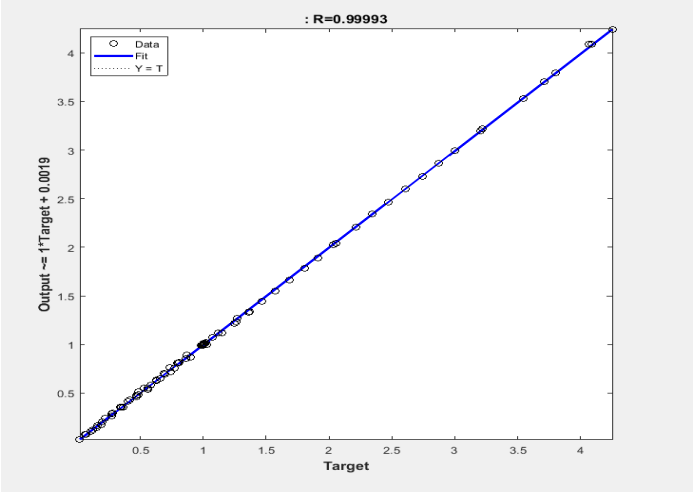


**Figure 15. ANN Training Regression Plot**

## 5.0 Conclusion

Transient stability study was performed on Benin 330kV sub grid network to determine the critical clearing angle and critical clearing time of the circuit breaker using artificial neural network technique known as Fletcher-Reeves back propagation algorithm. The swing equation was computed using Modified Euler's method. Based on the finding, it is here by concluded that transient stability was improved with the use of circuit breaker for fault clearance also artificial neural network technique shows greater potential for plaining and control of power system due to their ability to solve complex solution accurately and faster.

## References

Bashar, S.A. & Chin, K.G. (2016). Power system frequency stability and control: Survey. *International Journal of Applied Engineering Research*, *11*(8), 5688-5695.

Enemuoh, F.O (2012). *Simulation modelling of voltage stability of an interconnected electric power system network* (Ph.D Thesis). University of Nigeria, Nsuka.

Gupta, B.R. (2006). *Power system analysis and design*. Allahabard: Wheeler publishing.

Haque M.H. & Rahim A. (2012). Determination of first swing stability limit of multi machine power systems through Taylors series expansion. *IEE proceedings, 136*, 373-380.

Odia, A. (2007). *Transient stability assessment of the Nigerian 330kV network* (Master dissertation). University of Port Harcourt, Nigeria.

Prabha, K., Joh, P., Venkat, A., Goran, A., & Anjab, B. (2004). Definition and classification of power system stability. *IEEE Transaction on Power System, 19*(2), 1387-1401.

Rastgoufard S. (2018). *Applications of artificial intelligence in power system*. University of New Orleans. Thesis and Dissertation 2487.

Schlabbach, J. & Rafalski, K. (2008). *Power system engineer: Planning, design and operation of power systems and equipment*. University of Applied science, Bielefeld.

Stevenson, W.D. (2018). *Power System Analysis*. New Delhi: McGraw Hill.

Wood, A.J. & Wollenberg, B.F. (2016). Power generation operation. *WSEAS Transaction on Power Systems*, *17*, 12-17.